Developmental changes and injury induced disruption of the radial organization of the cortex in the immature rat brain revealed by in vivo diffusion tensor MRI

Sizonenko, Stéphane; Camm, Emily J; Garbow, Joel R; Maier, Stephan E; Inder, Terrie E; Williams, Chris E; Neil, Jeffrey J; Hüppi, Petra Susan

How to cite

SIZONENKO, Stéphane et al. Developmental changes and injury induced disruption of the radial organization of the cortex in the immature rat brain revealed by in vivo diffusion tensor MRI. In: Cerebral cortex, 2007, vol. 17, n° 11, p. 2609–2617. doi: 10.1093/cercor/bhl168

This publication URL: https://archive-ouverte.unige.ch/unige:44394

Publication DOI: 10.1093/cercor/bhl168

Cerebral Cortex November 2007;17:2609-2617
doi:10.1093/cercor/bhl168
Advance Access publication January 27, 2007

Developmental Changes and Injury Induced Disruption of the Radial Organization of the Cortex in the Immature Rat Brain Revealed by In Vivo Diffusion Tensor MRI

Stéphane V. Sizonenko[1], Emily J. Camm[1], Joel R. Garbow[2], Stephan E. Maier[3], Terrie E. Inder[2], Chris E. Williams[4], Jeffrey J. Neil[2] and Petra S. Huppi[1]

[1]Child Development Unit, Department of Paediatrics, School of Medicine, University of Geneva, Switzerland, [2]Mallinckrodt Institute of Radiology, Washington University Medical Centre, St Louis, USA, [3]Department of Radiology, Brigham's and Women's Hospital, Harvard Medical School, Boston, USA and [4]Liggins Institute, University of Auckland, Auckland, New Zealand

During brain development, morphological changes modify the cortex from its immature radial organization to its mature laminar appearance. Applying in vivo diffusion tensor imaging (DTI), the microstructural organization of the cortex in the immature rat was analyzed and correlated to neurohistopathology. Significant differences in apparent diffusion coefficient (ADC) and fractional anisotropy (FA) were detected between the external (I–III) and deep (IV–VI) cortical layers in postnatal day 3 (P3) and P6 pups. With cortical maturation, ADC was reduced in both cortical regions, whereas a decrease in FA was only seen in the deep layers. A distinct radial organization of the external cortical layers with the eigenvectors perpendicular to the pial surface was observed at both ages. Histology revealed maturational differences in the cortical architecture with increased neurodendritic density and reduction in the radial glia scaffolding. Early DTI after hypoxia–ischemia at P3 shows reduced ADC and FA in the ipsilateral cortex that persisted at P6. Cortical DTI eigenvector maps reveal microstructural disruption of the radial organization corresponding to regions of neuronal death, radial glial disruption, and astrocytosis. Thus, the combined use of in vivo DTI and histopathology can assist in delineating normal developmental changes and postinjury modifications in the immature rodent brain.

Keywords: brain development, cortex, diffusion tensor imaging, hypoxia–ischemia, rat

Introduction

Cerebral cortical organization is the result of complex and well-ordered events during cortical plate development. Cortical neurons are produced in a specific subventricular zone near the cerebral ventricles and also in a discrete ventricular zone deep to the subventricular zone and migrate to their appropriate position in the cerebral mantle (Brazel et al. 2003). Neocortical migrating neurons can adopt different types of trajectories. A large proportion of neurons migrate radially, along radial glia guides, from the germinative zone to the cortical plate. Others migrate from the ganglionic eminence, initially parallel to the pial surface along the deep white matter tracts, and then enter the developing cortex by following the radially oriented scaffolding of the radial glia cells, arriving at their final destination in the fetal cortical plate and assuming a well-defined, radially oriented, columnar organization (Rakic 1972, 1988; Sidman and Rakic 1973).

Subsequently, neuronal maturation involves growth of dendrites and axons with initiation of connectivity through intense synaptic formation. This phase is followed by pruning of synaptic connections with selective eliminations of cell populations (Sidman and Rakic 1973; Rakic 1982, 1988). In addition, bipolar radially orientated oligodendrocyte progenitors mature into highly branched oligodendrocytes with processes ensheathing axons for myelination while radial glia involutes (Hardy and Friedrich 1996). These developmental changes in cellular morphology lead to modification of the developing cortex from an immature radial to the mature laminar organization. Until now, ex vivo techniques such as electron microscopy, autoradiography, and immunohistology have been used to study the morphological and biochemical processes involved in cortical development (Cowan et al. 1997). Studies on human brain development have usually been done on postmortem tissue using traditional histological methods (Sidman and Rakic 1973; Honig et al. 1996; Volpe 2001) and more recently with magnetic resonance imaging (MRI) of fixed tissue or in vitro analysis of living brain slices (Letinic and Rakic 2001; Kostovic et al. 2002; Letinic et al. 2002). Recently, with the development of advanced MRI techniques, such as diffusion tensor imaging (DTI) or 3-dimensional volumetric MRI, it has been possible to evaluate normal and pathological human brain development in vivo (Huppi, Warfield, et al. 1998; Inder and Huppi 2000; McKinstry et al. 2002; Sbarbati et al. 2004). These techniques have also been used in animal research to study normal and pathological brain development using brain injury models or genetically modified animals (Mori et al. 2001; Zhang et al. 2003, 2005).

In the present study, we have evaluated the early postnatal patterning of cortical development in live rat pups using DTI. DTI is a technique that measures the movement of water within tissue and is sensitive to water molecule displacement on the order of 10 μm. This molecular motion is referred to as the "apparent diffusion" of water in recognition of the fact that water motion in tissue may reflect processes in addition to stochastic, thermally driven Brownian motion (McKinstry et al. 2002; Neil et al. 2002). DTI incorporates a measure of the directional dependence of water diffusion. For free water, apparent diffusion coefficient (ADC) values are equivalent in all directions (i.e., isotropic). In organized tissue such as white matter, water ADC values are not the same in all directions; they are greater parallel to fiber tracts than orthogonal to them (i.e., diffusion is anisotropic). The presence of diffusion anisotropy, with a preferred direction of water displacement, provides information about tissue microstructure. In the case of white matter, it indicates the orientation of fiber tracts. Overall, 3 parameters are typically calculated from DTI data: the directionally averaged water ADC, the degree of anisotropy of water diffusion (fractional anisotropy [FA]), and the orientation along which water apparent diffusion is maximal, represented by the orientation of the major eigenvector of the diffusion tensor. ADC is high and FA low in tissue with a high water content or when restriction to water movements is low due to widely spaced cellular elements. In human newborn cerebral cortex, water diffusion is anisotropic transiently during development (Neil et al. 1998) and has been suggested to reflect the radial

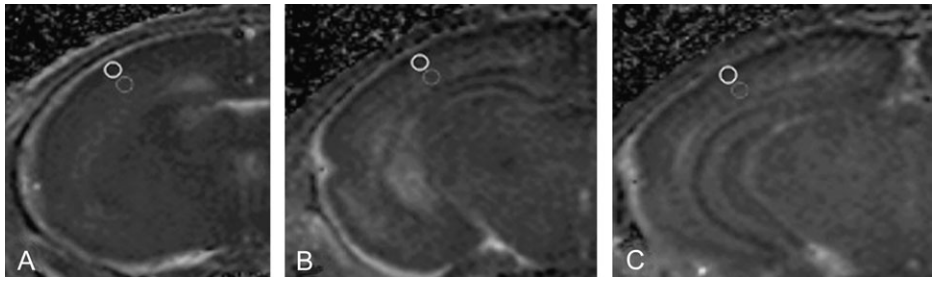

Figure 1. Cortical regions of interest for ADC and FA measures. ADC and FA were measured in the external (light gray circle) and internal layers (dark gray circle) of the parietal cortex at the level of the striatum (*A*), the dorsal hippocampus (*B*), and the ventral hippocampus (*C*).

organization of the developing cortex (McKinstry et al. 2002; Maas et al. 2004). This has also been demonstrated in post-mortem ex vivo studies in mouse (Mori et al. 2001; Zhang et al. 2003, 2005) and primate brains (Kroenke et al. 2005).

To study the effect of brain injury on in vivo DTI parameters in the developing brain, we have used a moderate hypoxic–ischemic (HI) injury in the postnatal day 3 (P3) rat brain that leads to selective neuroaxonal damage in the parietal cortex during the initial 12–24 h after the injury. Astrogliotic, microglial, and oligodendroglial reactions are present during this time and persist for weeks after the initial injury (Sizonenko and Kiss 2004; Sizonenko et al. 2005). These early events contribute to the loss of cortical volume and disruption of myelination seen at P21 in this model (Sizonenko et al. 2003). The changes described in this model after moderate HI injury in the P3 immature brain are comparable to some neuropathological features of diffuse brain injury seen in preterm infants. In this study, in order to evaluate intracortical maturation during early postnatal development, we have characterized water diffusion in live neonatal rat pups at P3 and P6 and compared it with subsequent specific histological assessment. Further, the effect of HI injury on water diffusion and microstructure in the developing cortex was investigated 24 and 72 h after HI.

Material and Methods

Animals

The Washington University Animal Studies Committee approved this study. Three days old Wistar rat pups from 3 different litters were used. As described previously (Sizonenko et al. 2003), rat pups underwent moderate HI injury. Briefly, the right carotid was ligated under halothane anesthesia, and the pups underwent hypoxia at 6% O_2 for 30 min at 37 °C. Twenty-four hours after HI injury ($n = 7$) or 3 days after HI ($n = 4$), each animal underwent an MRI study after which the brain was collected for histological examination. Prior to the imaging experiments, the rats were anesthetized with isoflurane/O_2 (4% v/v) and were maintained on isoflurane/O_2 (1.5% v/v) throughout the image acquisition under a thermoneutral environment.

MRI and Analysis

MRI was performed in an Oxford Instruments 4.7-T animal magnet equipped with 15-cm gradient coils. The data were collected using a 2-cm birdcage radio frequency coil. DTI data were acquired using a conventional spin echo imaging sequence, modified by the addition of a Stejskal–Tanner diffusion-sensitizing gradient pair. Six images with different gradient directions were acquired with a b value of 763 s/mm^2, together with a reference spin echo ($b = 0$) image. Other experimental parameters were $\Delta = 20$ ms, $\delta = 10$ ms, time repetition = 1.5 s, time echo = 0.04 s, slice thickness = 0.5 mm, field of view = 1.6 cm, matrix 128. Scanning time was 4 h. One pup from the P3 group died during the imaging and was subsequently excluded from the analysis. The geometric nature of the diffusion tensor can be used to display the architecture of the developing cortex. The diffusion tensor was calculated according to Basser and Pierpaoli (1996): the eigenvector associated with the largest eigenvalue was referred to as the primary eigenvector. The eigenvector with the maximum diffusion describes the direction along which maximum diffusion occurs, whereas the eigenvector with the minimum diffusion represents the direction with the least diffusion. ADC and FA were calculated using XPhase 1.16 software (Huppi, Maier, et al. 1998; Huppi et al. 2001). Regions of interest were in the deep (IV–VI) and superficial layers (I–III) of the left uninjured parietal cortex at the level of the striatum, dorsal hippocampus, and ventral hippocampus (Fig. 1). These areas showed specific water diffusion characteristics in the developing mouse brain (Mori et al. 2001). The orientations of the major eigenvectors were calculated and displayed using XPhase 1.16 software (Huppi, Maier, et al. 1998; Huppi et al. 2001). No significant differences in ADC and FA were seen between the 3 rostrocaudal levels analyzed (Fig. 1). Therefore, the mean deep and external ADC/FAs for the 3 brain levels at P3 and P6 were compared using a Wilcoxon test. A $P < 0.05$ was considered statistically significant. To assess the effect of HI injury on ADC and FA, contralateral and ipsilateral ADC/FAs at 24 and 72 h after injury were measured in the deep layers of the parietal cortex at the level of the dorsal hippocampus. Only the deep layers have been investigated in the HI group as the damage resulting from the HI insult lies in these layers as previously described (Sizonenko et al. 2003, 2005). Only the brains showing histological injury in the parietal cortex were compared with a paired t-test. Again, $P < 0.05$ was considered statistically significant.

Histology

After MRI acquisition, the pups were sacrificed. Intracardiac perfusion of NaCl 0.9% was followed by tissue fixation with 4% paraformaldehyde in 0.1% phosphate-buffered saline (PBS). The brain was collected and processed in increasing concentrations of ethanol and embedded in paraffin. Contiguous 4-μm sections at the level of the striatum and dorsal hippocampus were cut on a microtome (Leica, Wetzlar, Germany) and collected on Polysin® (Menzel-Glaser, Braunscheig, Germany) slides. Conventional hematoxylin–eosin (HE) staining was used to demonstrate cortical architecture and injury. Fluoro-Jade B (FJB), which has been employed to detect degenerating neurons and axons in a number of neuronal injury models (Schmued and Hopkins 2000; Sizonenko et al. 2005), was used to assess neuroaxonal degeneration. Following the protocol used by Schmued and Hopkins (2000), the sections were stained with FJB (Histo-Chem Inc., Jefferson, AR) and 4′,6′-diamidino-2-phenyllindole (Sigma, St Louis, MO).

For specific immunohistology of glial cells and neurons, a litter that did not have an MRI scan was used and underwent HI injury at P3. The brains were collected at 24 and 72 h after HI. Brains were fixed with 4% paraformaldehyde in 0.9% NaCl and immersed in 30% sucrose before being frozen. Immunostaining for nestin (a marker of radial glial cells; Kalman and Ajtai 2001) and glial fibrillary acidic protein (GFAP-a marker of activated astrocytes; Kalman and Ajtai 2001) was performed: 20 μm fixed frozen sections at the level of the dorsal hippocampus were collected onto gelatine-coated slides. Nonspecific binding was blocked by incubating the slides in PBS containing 2.5% normal goat serum and 1% bovine serum albumin (BSA) for 30 min at room temperature. They were then incubated with the different primary antibody for nestin (1:1000, MAB353, Chemicon, Temecula, CA) or GFAP (1:400, Z334, Dako, Glostrup, Denmark) in PBS–Tris overnight at 4 °C. This was

followed with a 60-min incubation at room temperature with Alexa 555 anti-mouse (1:200) and Alexa 488 anti-rabbit (1:200) secondary antibodies, respectively (Molecular Probes, Invitrogen, Paisley, UK). Slides were rinsed in PBS and mounted using PBS–Glycine media. For neurodendritic visualization, microtubule-associated protein 2 (MAP2, 1:100, MAB 3418, Chemicon International) was used. Activity of endogenous peroxidases was blocked with 0.3% H_2O_2 in methanol for 20 min. Nonspecific binding was blocked by incubating the slides in 4% BSA for 1 h at room temperature. Sections were incubated in primary antibody for 24 h at 4 °C. This was followed with 60-min incubations at room temperature in secondary antibody (1:200 anti-mouse immunoglobulin G; Vectastain kit, Vector Laboratories, Burlingame, CA) and the avidin–biotin complex (1:200, Vector Laboratories). Sections were then developed with the chromagen, 3,3′ diaminobenzidine–Nickel, containing hydrogen peroxide for 10 min.

Microscopy

For Nestin quantification, sections were systematically examined with an epifluorescent microscope using rhodamine filters. Image acquisition was performed using a Nikon digital camera and dedicated software. To examine the proportion of the cortex occupied by radial glia, 3 sections at the level of the dorsal hippocampus were examined from each animal, at a magnification of 40×. From each hemisphere, 2 fields within the cortex were selected for sampling, at the external and internal layers. A grid (0.01 mm^2) was placed over the section, and the number of radial glia that fell within the grid was counted within both fields. Results from each animal were pooled, and a mean value was calculated. Quantitative analysis of the density and length of blood vessels was performed on nestin-stained sections. Two randomly selected areas in both the deep and external layers of the cortex were sampled, respectively. A grid (0.09 mm^2) was placed over the section at 100× magnification, and the density of blood vessels, as well as the number of blood vessels that intersected the grid, were counted. The values for each animal were pooled and a mean of means calculated for each age group. For neuronal and dendritic density, bright field illumination was used, and digital pictures of MAP2-stained sections of the parietal cortex at the level of the dorsal hippocampus were taken. Using ImageJ V1.34l for MacOSX (National Institutes of Health), optical density (OD) was measured in 4 distinct areas in the deep and external cortical layers corresponding to the ADC and FA measurements. Three sections per animal were measured; the mean of all measurements for each specific cortical level was used. The effects of HI on nestin-positive radial glial fibers were assessed in both the area of the lesion and in the contralateral (undamaged) hemisphere, using MetaMorph® Imaging System (Meta Imaging Software, Molecular Devices Corporation, Pennsylvania). To assess the degree of disruption of the radial orientation (perpendicular to the pial surface) of the nestin-positive cells, we have measured the number and length of nestin-positive cell structure that remained within this orientation after HI. Preliminary analysis revealed that 50% of nestin-positive fibers were orientated 15° either side of the main radial orientation; therefore, we assessed the number and total length of nestin-positive radial glial fibers within these limits of radial orientation. The main positive nestin elements that did not fall within the ±15° orientation included blood vessels and their ramifications. Two to 4 sections per animal were analyzed; values for each animal were pooled and a mean value calculated. A mean of means ± standard error of mean was calculated for each group. Colocalization for Nestin and GFAP was performed on LSM 510 (Zeiss, Feldbach, Switzerland) confocal microscopy system. All measures were made on coded slides, with the code not being broken until all measurements were made. Nestin and MAP2 values in the deep and external layers were compared using a *T*-test. A $P < 0.05$ was considered statistically significant.

Results

Diffusion Changes Reflect Cortical Maturation

In the P3 rat, ADC measured in the deep cortical layers (960 ± 100 $\mu m^2/s$) was significantly higher compared with the one in the external cortical layers (750 ± 100 $\mu m^2/s$) in the 3 anterior, mid, and posterior levels of the brain (Fig. 2*A*). FA measured in the deep cortical layers (0.29 ± 0.06) was significantly lower compared with the one in the external layers (0.39 ± 0.05) (Fig. 2*B*). Similarly, ADC values were significantly higher in the deep cortical layers at P6 (830 ± 1 00 $\mu m^2/s$) compared with the external cortical layers (580 ± 110 $\mu m^2/s$) (Fig. 2*A*). FA was significantly lower in the deep cortical layers (0.21 ± 0.02) compared with the external layers (0.36 ± 0.07) (Fig. 2*B*). ADC values were significantly reduced in both cortical deep and external levels at P6 compared with P3 (Fig. 2*A*). A significant decrease in FA was present in the deep cortical layer between P3 and P6 animals (Fig. 2*B*), whereas no difference was present in the superficial cortical layers. Overlaid DTI maps showing the orientation of the major eigenvector revealed a radial organization of the external cortical layers, with the eigenvectors being perpendicular to the pial surface. In the deep layers, this radial pattern was not as prominent. Fewer eigenvectors perpendicular to the pial surface were present in the deep cortical layers in the P6 rats compared with P3 (Fig. 3).

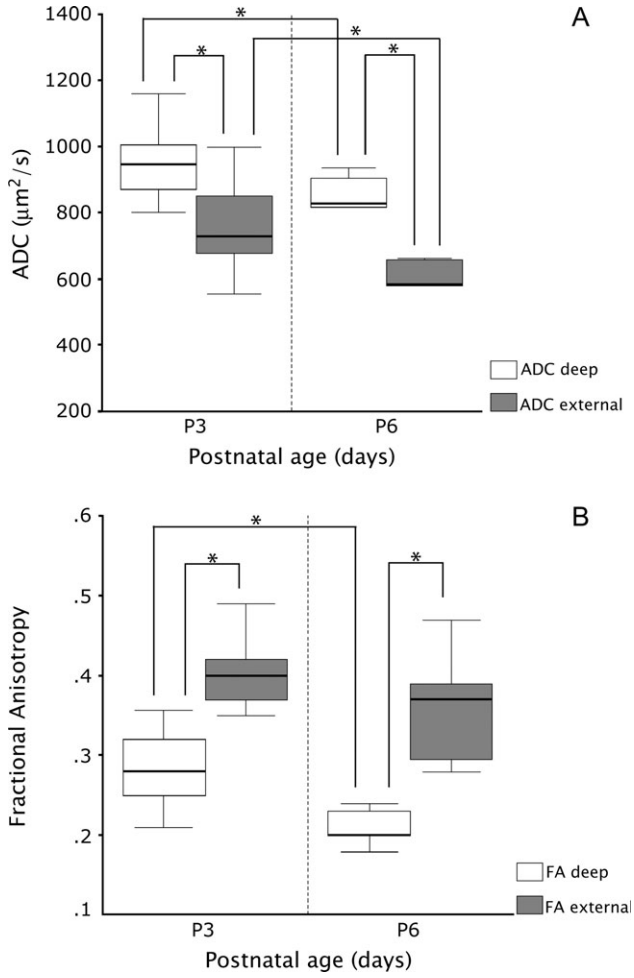

Figure 2. Cortical ADC and FA during development: (*A*) Boxplot of ADC values measured in the external and deep cortex at P3 and P6. (*B*) Boxplot of FA values measured in the external and deep cortex at P3 and P6. * = $P < 0.05$.

On conventional HE histological sections at P3 and P6, the deep layers showed lower cellularity compared with the external layers. Histological differences between P3 and P6 were not detected with conventional HE staining. However, using MAP2 immunostaining, differences in the deep and external layers were detected. At both ages, MAP2 immunoreactivity appeared less intense in the deep layers compared with

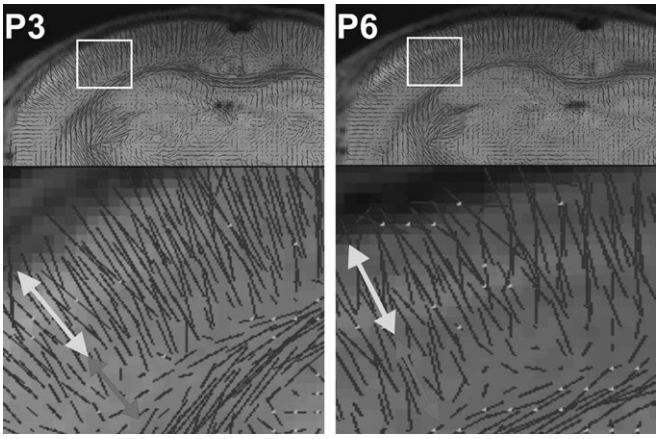

Figure 3. Eigenvectors overlaid on coronal DTI from a P3 and P6 rat. The orientation and the density of the fibers are shown by the indicated vectors, and the degree of anisotropy is symbolized by the vector length. Fibers that are perpendicular to the image plane are distinguished by the clear dots. At both ages, the radial organization of the cortex is depicted by the eigenvectors being perpendicular to the pial surface. The insets show a magnification of the parietal cortex. At P3 (left panel), the radial organization is clearly present, whereas at P6, (right panel) the radial orientation of the eigenvectors is less prominent, especially in the deep layers. The white and gray arrows correspond, respectively, to the external layers and to the deeper layers of the cortex where ADC and FA measures were made (see Fig. 1).

the external layers. Furthermore, a radial organization of neuronal processes could be seen in the external layers especially at P3, with a modification of this pattern at P6 (Fig. 4*A,B*). The OD of MAP2 was significantly lower in the deep layers (0.38 ± 0.029) compared with the external ones (0.53 ± 0.035) in the P3 rat pup. Similarly, At P6, OD of MAP2 was lower in the deep layers of the cortex (0.54 ± 0.027) compared with the external layers (0.69 ± 0.027) (Fig. 4*C*), indicating a lower neuronal and dendritic density within the deep layers. A significant increase in OD was present between P3 and P6 in both areas of cortical layers measured (Fig. 4*C*), indicating changes in neuronal structure.

Nestin immunoreactivity revealed the radial glia scaffolding that extends from the corpus callosum to the external cortical layers (Fig. 4*D,E*). In the P3 rat, the radial glia cells appeared as a regular and dense pattern of parallel fibers perpendicular to the pial surface extending through the immature cortex. Nestin-positive blood vessels were also present. Fewer radial glia cells were present at P6 compared with P3, and the fiber pattern was less dense and less organized (Fig. 4*D,E*). In the P3 pups, nestin-positive cells were significantly less in the deep layers (25.95 ± 1.03 per 10 μm^2) compared with the external layers (36.5 ± 1.36 per 10 μm^2) (Fig. 4*F*). Similarly at P6, significantly less nestin-positive cells were seen in the deep layers (17.0 ± 1.38 per 10 μm^2) compared with the external (28.48 ± 1.76 per 10 μm^2) (Fig. 4*F*). A significant reduction in nestin-positive radial glial cells was also present within each cortical depth between P3 and P6, indicating a rapid reduction of the radial glia with age (Fig. 4*F*). The number and length of blood vessels were significantly lower in the deep layers compared with the external layers, but no difference with age was detected (data not shown).

Diffusion Changes and Microstructure Disruption Reflect Neuronal Degeneration and Modification of Glia after HI Injury

Twenty-four hours after HI injury, ADC values in the deep layers of the ipsilateral cortex (805 ± 24 $\mu m^2/s$) were significantly lower compared with the contralateral cortex (832 ± 21 $\mu m^2/s$) (Fig. 5*A*). FA was significantly lower in the ipsilateral cortex (0.29 ± 0.01) compared with the contralateral (0.33 ± 0.01) (Fig. 5*B*). At 72 h, ADC and FA values in the ipsilateral cortex (836 ± 16 $\mu m^2/s$, 0.29 ± 0.01) were higher compared with the contralateral cortex (754 ± 19 $\mu m^2/s$; 0.27 ± 0.01) (Fig. 5*A,B*). In the ipsilateral cortex, ADC or FA at 24 and 72 h after HI injury did not show any statistically significant differences, whereas the contralateral cortex showed a significant decrease in ADC and FA (Fig. 5*A,B*). In the ipsilateral cortex, vector maps showed areas of disruption of the radial organization of the cortex, with reduction and random directionality of the major eigenvectors at both time points (Fig. 6*A*). HE staining revealed looser tissue structure in the damaged area, especially at 72 h. Furthermore, these areas of ADC change and disorganized eigenvector orientation corresponded to regions within the parietal cortex of neuronal injury stained with FJB 24 and 72 h after HI injury (Fig. 6*B*). In addition, at both time points, the number of nestin-positive radial glia cells was not different in the ipsilateral cortex compared with contralateral, but these radial glia cells showed histological transformation with disruption of the regular pattern, larger cell bodies, and thicker lateral processes (Fig. 7*A,B*). As described previously (Sizonenko et al. 2005), in the injured cortex, GFAP-positive astrocytes were also increased at both time points and showed morphology typical of activated astrocytes, with enlarged cell bodies and thicker processes compared with the contralateral cortex. Colocalization of nestin and GFAP immunostaining was present in the ipsilateral cortex, suggestive of radial glia transformation into astrocytes in response to the HI injury with formation of a glial scar (Fig. 7*C–E*). When assessing radial glia within the ±15° of the orientation perpendicular to the pial surface, the number of radially orientated nestin-positive fibers tended to be decreased in the right hemisphere compared with the left, 24 h after HI injury ($P = 0.063$). However, 24 h after HI, the total length of nestin-positive fibers was significantly reduced in the right hemisphere ($P < 0.05$). At 72 h after HI injury, both the number and total length ($P < 0.05$) were significantly reduced in the right hemisphere compared with the left (Fig. 7*F,G*).

Discussion

The radial organization of the neocortex is a fundamental microstructural feature of immature cortex and occurs in many species, including humans. In a distinct manner during brain development, there is a transition from the immature organization of the developing cortex to the mature organization of the adult cortex. In this report, we present the first data on in vivo DTI to study changes in the radial organization of early postnatal cortical development and its disruption by HI injury in an immature rat model. Changes in the ADC and FA of the neonatal rat cortex at P3 and P6 demonstrate a gradual disappearance of the radial organization with the deep layers maturing earlier than the external layers. This progression is correlated with cytoarchitectural changes present during early postnatal cortical development. These changes included increased MAP2 immunostaining, representative of neurodendritic development, and reduction of radial glial scaffolding documented by the loss of immunostaining for nestin between P3 and P6. These structural changes contribute to the changes of the immature radial organization of the cortex to the mature cortical organization.

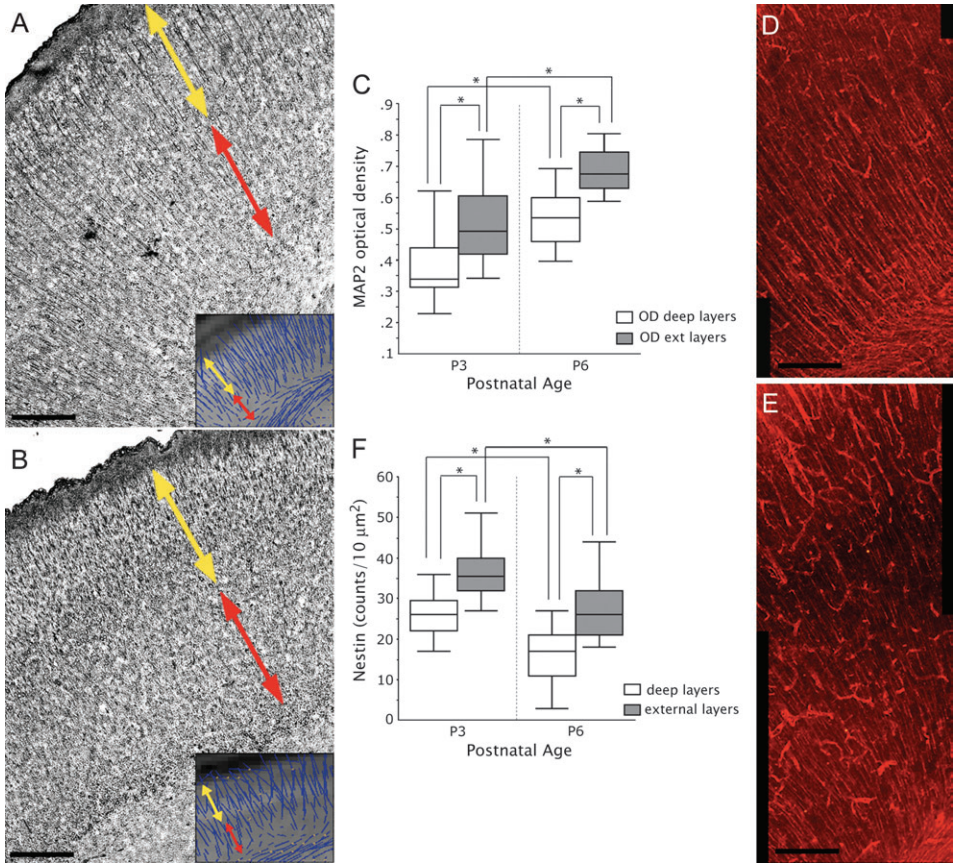

Figure 4. Immunohistochemical analysis of the cortex at P3 and P6: (*A*, *B*) Parietal cortex at P3 (*A*) and P6 (*B*) in the regions of interest of ADC and FA measurements stained with MAP2 to identify neurons and their processes. A higher cellular density is seen in the external layers (yellow arrows) compared with the deeper layers (red arrow) at both ages (scale bar = 500 μm). Radial organization of neuronal processes could be seen in the external layers at P3, with a reduction of this pattern at P6. (*C*) Boxplot showing the OD of MAP2 immunostaining in the deep and external cortical layers at both ages analyzed (* = $P < 0.05$). (*D*, *E*) Nestin immunostaining of radial glial cells in the parietal cortex at P3 (*D*) and P6 (*E*). The photomicrographs represent the full thickness of the cortex. At P3, a dense and regular pattern of radially oriented glial cells is present. At P6, the organization of the radial glia appears less dense and regular (scale bar = 100 μm). (*F*) Boxplot of nestin-positive cells in the deep and external layers of the cortex at P3 and P6 (* = $P < 0.05$).

Disruption of normal cortical development occurs after perinatal brain injury in the preterm infant and lies at the origin of cognitive deficits or mental retardation in this population (Inder et al. 1999; Woodward et al. 2005). Moderate HI at P3 is an ideal model to study early cortical injury and its effects on subsequent cortical development (Sizonenko et al. 2003). A moderate HI injury at P3 produced changes in water diffusion and anisotropy similar to acute injury in human studies, with subsequent alterations in cortical microstructure defined by DTI (Huppi et al. 2001). Loss of cortical anisotropy after injury was associated with the presence of degenerating neurons and foamy astrocytes with a marked disruption of radial glia present in the ipsilateral side. An understanding of what causes water diffusion changes in normal development or following HI and the relationship between DTI changes and the specific structural or chemical changes triggered by these events is likely to be multifactorial. Water diffusion properties are strongly influenced by tissue microstructure. In white matter, for example, diffusion anisotropy reflects the organization of myelinated white matter tracts (Beaulieu and Allen 1994). Whereas white matter tract development has been well studied using DTI (Huppi, Maier, et al. 1998; Neil et al. 1998; Mori et al. 2001; Miller et al. 2002), less is known about the DTI changes present in the developing cortex. There are several developmental events that occur in cortex that will influence water diffusion. The reduction in water content of the brain (Dobbing and Sands 1973; Kreis et al. 1993; Neil et al. 1998; Mukherjee et al. 2002), the expansion of dendritic trees (Marin-Padilla 1992), the increased ramification of oligodendrocytes (Rivkin et al. 1995; Back et al. 1996; Hardy and Friedrich 1996), and the reduction of the radial glia scaffolding (Rakic 2003a, 2003b) that takes place during postnatal cortical development are likely responsible for the decrease in water diffusion and anisotropy that we observe. Similar observations have been made in the developing brain of other animal species (Baratti et al. 1999; Mori et al. 2001; Kroenke et al. 2005) and humans (Kostovic et al. 2002; McKinstry et al. 2002; Maas et al. 2004). These changes appear to be similar in these species, despite differences in the organization of the cortex, that is, the subplate is prominent in the human cortex, and disappear with maturation, whereas in the rodent, the subplate appears less prominent and is suggested to remain present in adulthood as layer VII (Reep 2000; Robertson et al. 2000; Kostovic et al. 2002). Further, ADC and FA were different between the more mature deep layers and the immature external layers for both postnatal ages investigated. In the deep layers, ADC was higher and FA lower compared with the external layers. Histological examination revealed less cellularity and looser cortical cytoarchitectonics in the deep layers than the external layers. This effect was more pronounced at P3 than at P6. Similar differences in anisotropy

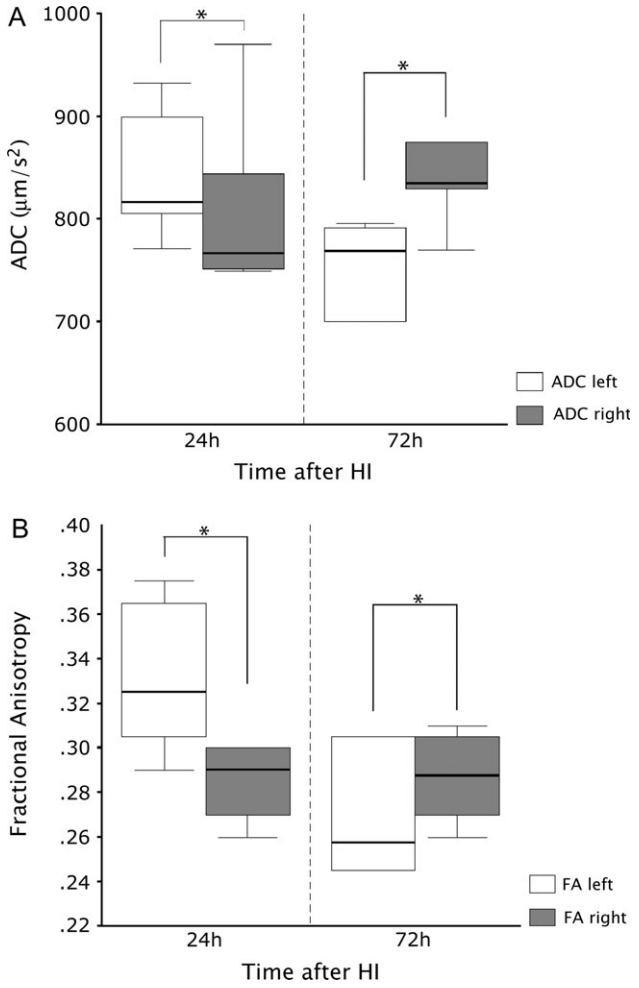

Figure 5. Combined ADC and FA of the external and deep cortical layers after HI injury: (*A*) Boxplot of cortical ADC values measured 24 and 72 h after HI. (*B*) Boxplot of cortical FA values measured 24 and 72 h after HI. * = $P < 0.05$.

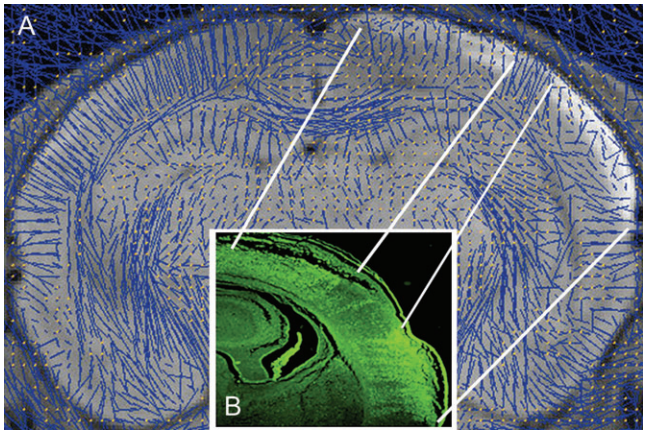

Figure 6. DTI and histological changes in the same animal 24 h after HI injury: (*A*) A disrupted pattern of eigenvectors 24 h after HI injury in the parietal cortex. (*B*) Degenerating neurons stained with FJB appear bright and correspond to the area of disorganized eigenvectors. Note that the area where the eigenvectors remain with a regular and radial pattern corresponds to a region with no neuronal degeneration detected with FJB.

between cortical layers have been described in the mouse brain (Mori et al. 2001). In the mouse, 3 cerebral layers could be separated on the basis of FA values and eigenvector directionality: the innermost layer of high anisotropy, an intermediate layer with lower anisotropy, and the external layer with high anisotropy. These 3 layers were assigned by the authors as the periventricular zone, the intermediate zone, and the cortical plate, respectively (Mori et al. 2001). With increasing postnatal age, anisotropy gradually decreased in the 2 external layers. The changes in regions of interest measured in our study are likely to correspond to the changes seen in the intermediate zone and in the cortical plate described in the mouse.

The high anisotropy observed in the deep and external layers of the cortex at P3 and the external layers at P6 showed a preferred directionality perpendicular to the cortical surface, as illustrated by the major eigenvector orientations. At this stage of development, neurons with radially oriented dendrites and axons as well as radial glial fibers are most likely responsible for the preferred direction of water diffusion being perpendicular to the cortical surface. With increasing postnatal age, a reduction in the consistency of orientation of the major eigenvectors was seen in association with a decrease of cortical FA. After neuronal migration is completed, a "cortical maturation" phase starts with progressive neuronal maturation that includes dendritic arborization, synapse formation (Sidman and Rakic 1973; Kostovic and Rakic 1990; Kostovic et al. 2002), and disappearance of the radial glia cells (Rakic 2003a, 2003b). In this study, nestin immunoreactivity was reduced at P6 compared with P3. These developmental events will alter the preferred direction of water motion by increasing the water diffusion parallel to cortical surface, thereby reducing overall anisotropy.

Pathological processes such as HI injury modify the integrity of the tissue microstructure and result in significant alteration in water diffusion parameters within damaged tissue. Using DTI, we have shown that, after a moderate HI injury in the P3 rat brain, an alteration in ADC and FA in the injured cortical gray matter is present and these changes can be correlated with neuronal death, radial glia disruption, and astrogliosis. In several studies of acute HI injury in young rats (Rumpel et al. 1995, 1997; Miyasaka et al. 2000), ADC was reduced in injured cortex following different patterns: 1) a transient decrease during the HI injury, 2) a biphasic pattern with normalization of the ADC 60 min after the end of HI but with a secondary reduction at 48 h, and 3) a continuous reduction of ADC up to 48 h. These patterns of ADC change were related to the severity of the injury on histopathology; with the less-damaged brains showing transient changes and more severely damaged ones showing continuous ADC reduction. In our P3-HI model, the ADC reduction at 24 h occurred at the peak of neuronal death illustrated by positive FJB staining, axonal degeneration, and astrocytic activation (Sizonenko et al. 2005). Seventy-two hours after HI injury, ADC and FA were both significantly increased compared with the contralateral cortex, in conjunction with persistent neuronal loss, radial glia disruption, and transformation into astrocytes. Interestingly, when comparing the injured cortices at both time points, no significant differences in the ADC and FA values were present. Thus, diffusion and anisotropy alterations detected by DTI remained similar at 24 and 72 h after HI in the injured cortex, whereas the contralateral noninjured cortex showed the reduction of both ADC and FA associated with normal cortical maturation. The important gliotic

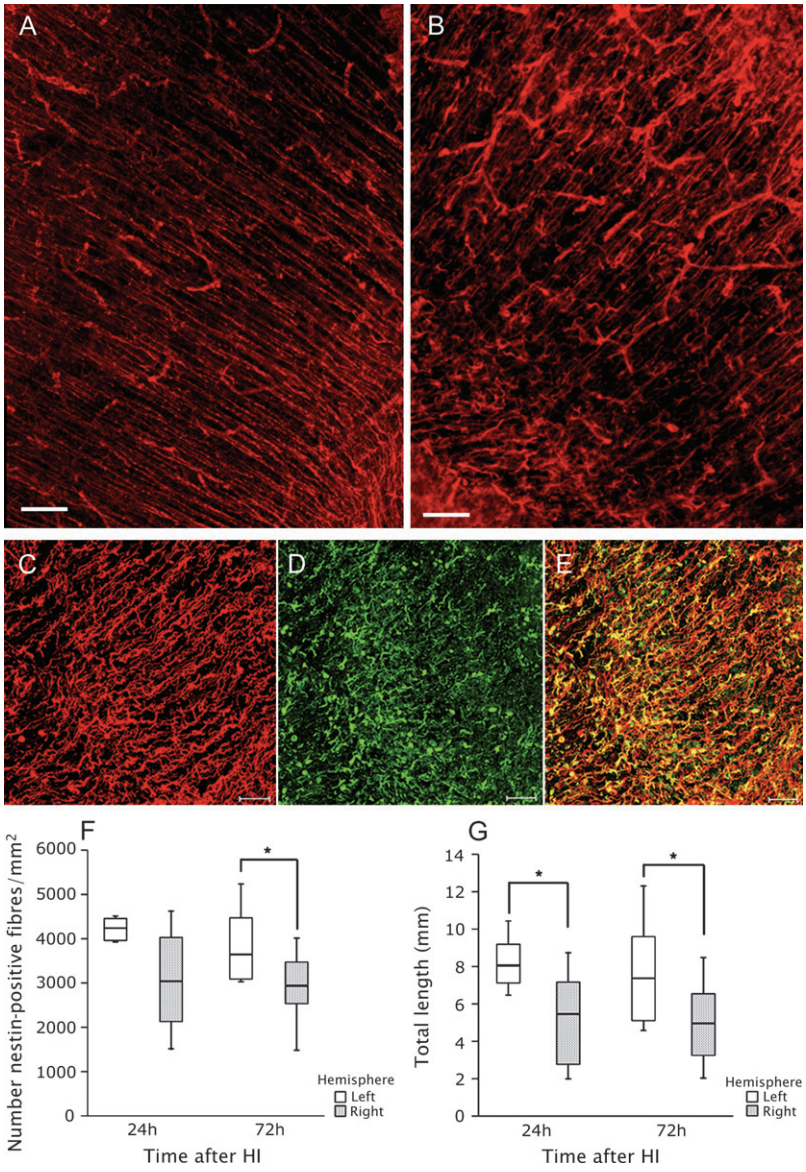

Figure 7. Immunostaining of nestin 24 h after HI injury (*A*, *B*): (*A*) Representative nestin immunostaining in the left, uninjured parietal cortex and in the right, injured cortex (*B*). Similar changes in radial glia were present at 72 h. Confocal imaging of nestin and GFAP 24 h after HI injury (*C*–*E*): (*C*) Disrupted nestin-positive radial glia; (*D*) Increased GFAP immunostaining in the area of injury with hypertrophic foamy astrocytes; (*E*) Colocalization of nestin and GFAP (scale bars: 50 μm). Quantification of radial glia morphometric changes (*F*, *G*): (*F*) Boxplots of the number of radially orientated nestin-positive radial glial fibers in the left and right hemispheres at 24 and 72 h following HI injury. (*G*) Boxplots of the total cumulative length of radially orientated nestin-positive glial fibers in the left and right hemispheres at 24 and 72 h following HI injury. (* = $P < 0.05$).

reaction—including radial glia disruption, hypertrophic astrocytes, and microglia activation that characterize the developing brain after HI—is present in the injured cortex and results in the formation of gliotic scars (Sizonenko et al. 2003, 2005). Similarly, at 72 h, the persistent gliotic reaction with hypertrophic astrocytes, radial glia alteration, and microglia activation in the injured cortex will modify tissue microstructure resulting in differences in ADC and FA compared with the normal maturing contralateral cortex. Therefore, the alterations in ADC and FA seen 72h after HI are likely and partly due to the intense glial reaction that is following the injury, in addition to neuronal cell death.

In conclusion, we have shown that in vivo DTI can detect microstructural changes during early cortical development and that these alterations are related to histological modifications in the postnatal rat cortex. Moderate HI injury to the immature rodent brain leads to acute alterations in cytoarchitectonic organization of the developing cortex that manifest as changes in DTI parameters. These findings confirm that DTI is a very useful tool not only to assess normal brain development but also to assess acute and long-term postinjury plasticity and, more importantly, the potential effects of neuroprotective interventions on cerebral microstructure organization.

Notes

This work was supported by National Research Centre for Growth and Development-New Zealand and by the Schmiedheiny and Boninchi and Von Meissner Foundations, Geneva, Switzerland. SVS was recipient of a Fellowship from the Geneva University Hospital. *Conflict of Interest*: None declared.

Address correspondence to Dr Stéphane V. Sizonenko, Unité de Développement, Hôpital des Enfants, 6 rue Willy Donzé, 1211 Geneva 14, Switzerland. Email: stephane.sizonenko@medecine.unige.ch.

References

Back SA, Kinney HC, Volpe JJ. 1996. Immunocytochemical characterization of oligodendrocyte development in human cerebral white matter. Soc Neurosci. 20:A1722.

Baratti C, Barnett AS, Pierpaoli C. 1999. Comparative MR imaging study of brain maturation in kittens with T1, T2, and the trace of the diffusion tensor. Radiology. 210:133–142.

Basser PJ, Pierpaoli C. 1996. Microstructural and physiological features of tissues elucidated by quantitative-diffusion-tensor MRI. J Magn Reson B. 111:209–219.

Beaulieu C, Allen PS. 1994. Determinants of anisotropic water diffusion in nerves. Magn Reson Med. 31:394–400.

Brazel CY, Romanko MJ, Rothstein RP, Levison SW. 2003. Roles of the mammalian subventricular zone in brain development. Prog Neurobiol. 69:49–69.

Cowan W, Zipursky S, Jessel T. 1997. Molecular and cellular approaches to neural development. New York: Oxford University Press.

Dobbing J, Sands J. 1973. Quantitative growth and development of human brain. Arch Dis Child. 48:757–767.

Hardy RJ, Friedrich VL Jr. 1996. Progressive remodeling of the oligodendrocyte process arbor during myelinogenesis. Dev Neurosci. 18:243–254.

Honig LS, Herrmann K, Shatz CJ. 1996. Developmental changes revealed by immunohistochemical markers in human cerebral cortex. Cereb Cortex. 6:794–806.

Huppi PS, Maier SE, Peled S, Zientara GP, Barnes PD, Jolesz FA, Volpe JJ. 1998. Microstructural development of human newborn cerebral white matter assessed in vivo by diffusion tensor magnetic resonance imaging. Pediatr Res. 44:584–590.

Huppi PS, Murphy B, Maier SE, Zientara GP, Inder TE, Barnes PD, Kikinis R, Jolesz FA, Volpe JJ. 2001. Microstructural brain development after perinatal cerebral white matter injury assessed by diffusion tensor magnetic resonance imaging. Pediatrics. 107:455–460.

Huppi PS, Warfield S, Kikinis R, Barnes PD, Zientara GP, Jolesz FA, Tsuji MK, Volpe JJ. 1998. Quantitative magnetic resonance imaging of brain development in premature and mature newborns. Ann Neurol. 43:224–235.

Inder TE, Huppi PS. 2000. In vivo studies of brain development by magnetic resonance techniques. Ment Retard Dev Disabil Res Rev. 6:59–67.

Inder TE, Huppi PS, Warfield S, Kikinis R, Zientara GP, Barnes PD, Jolesz F, Volpe JJ. 1999. Periventricular white matter injury in the premature infant is followed by reduced cerebral cortical gray matter volume at term. Ann Neurol. 46:755–760.

Kalman M, Ajtai BM. 2001. A comparison of intermediate filament markers for presumptive astroglia in the developing rat neocortex: immunostaining against nestin reveals more detail, than GFAP or vimentin. Int J Dev Neurosci. 19:101–108.

Kostovic I, Judas M, Rados M, Hrabac P. 2002. Laminar organization of the human fetal cerebrum revealed by histochemical markers and magnetic resonance imaging. Cereb Cortex. 12:536–544.

Kostovic I, Rakic P. 1990. Developmental history of the transient subplate zone in the visual and somatosensory cortex of the macaque monkey and human brain. J Comp Neurol. 297:441–470.

Kreis R, Ernst T, Ross BD. 1993. Development of the human brain: in vivo quantification of metabolite and water content with proton magnetic resonance spectroscopy. Magn Reson Med. 30:424–437.

Kroenke CD, Bretthorst GL, Inder TE, Neil JJ. 2005. Diffusion MR imaging characteristics of the developing primate brain. Neuroimage. 25:1205–1213.

Letinic K, Rakic P. 2001. Telencephalic origin of human thalamic GABAergic neurons. Nat Neurosci. 4:931–936.

Letinic K, Zoncu R, Rakic P. 2002. Origin of GABAergic neurons in the human neocortex. Nature. 417:645–649.

Maas LC, Mukherjee P, Carballido-Gamio J, Veeraraghavan S, Miller SP, Partridge SC, Henry RG, Barkovich AJ, Vigneron DB. 2004. Early laminar organization of the human cerebrum demonstrated with diffusion tensor imaging in extremely premature infants. Neuroimage. 22:1134–1140.

Marin-Padilla M. 1992. Ontogenesis of the pyramidal cell of the mammalian neocortex and developmental cytoarchitectonics: a unifying theory. J Comp Neurol. 321:223–240.

McKinstry RC, Mathur A, Miller JH, Ozcan A, Snyder AZ, Schefft GL, Almli CR, Shiran SI, Conturo TE, Neil JJ. 2002. Radial organization of developing preterm human cerebral cortex revealed by non-invasive water diffusion anisotropy MRI. Cereb Cortex. 12:1237–1243.

Miller SP, Vigneron DB, Henry RG, Bohland MA, Ceppi-Cozzio C, Hoffman C, Newton N, Partridge JC, Ferriero DM, Barkovich AJ. 2002. Serial quantitative diffusion tensor MRI of the premature brain: development in newborns with and without injury. J Magn Reson Imaging. 16:621–632.

Miyasaka N, Nagaoka T, Kuroiwa T, Akimoto H, Haku T, Kubota T, Aso T. 2000. Histopathologic correlates of temporal diffusion changes in a rat model of cerebral hypoxia/ischemia. Am J Neuroradiol. 21:60–66.

Mori S, Itoh R, Zhang J, Kaufmann WE, van Zijl PC, Solaiyappan M, Yarowsky P. 2001. Diffusion tensor imaging of the developing mouse brain. Magn Reson Med. 46:18–23.

Mukherjee P, Miller JH, Shimony JS, Philip JV, Nehra D, Snyder AZ, Conturo TE, Neil JJ, McKinstry RC. 2002. Diffusion-tensor MR imaging of gray and white matter development during normal human brain maturation. Am J Neuroradiol. 23:1445–1456.

Neil J, Miller J, Mukherjee P, Huppi PS. 2002. Diffusion tensor imaging of normal and injured developing human brain—a technical review. NMR Biomed. 15:543–552.

Neil JJ, Shiran SI, McKinstry RC, Schefft GL, Snyder AZ, Almli CR, Akbudak E, Aronovitz JA, Miller JP, Lee BC, et al. 1998. Normal brain in human newborns: apparent diffusion coefficient and diffusion anisotropy measured by using diffusion tensor MR imaging. Radiology. 209:57–66.

Rakic P. 1972. Mode of cell migration to the superficial layers of fetal monkey neocortex. J Comp Neurol. 145:61–83.

Rakic P. 1982. Early developmental events: cell lineages, acquisition of neuronal positions, and areal and laminar development. Neurosci Res Program Bull. 20:439–451.

Rakic P. 1988. Specification of cerebral cortical areas. Science. 241:170–176.

Rakic P. 2003a. Developmental and evolutionary adaptations of cortical radial glia. Cereb Cortex. 13:541–549.

Rakic P. 2003b. Elusive radial glial cells: historical and evolutionary perspective. Glia. 43:19–32.

Reep RL. 2000. Cortical layer VII and persistent subplate cells in mammalian brains. Brain Behav Evol. 56:212–234.

Rivkin MJ, Flax J, Mozell R, Osathanondh R, Volpe JJ, Villa-Komaroff L. 1995. Oligodendroglial development in human fetal cerebrum. Ann Neurol. 38:92–101.

Robertson RT, Annis CM, Baratta J, Haraldson S, Ingeman J, Kageyama GH, Kimm E, Yu J. 2000. Do subplate neurons comprise a transient population of cells in developing neocortex of rats? J Comp Neurol. 426:632–650.

Rumpel H, Buchli R, Gehrmann J, Aguzzi A, Illi O, Martin E. 1995. Magnetic resonance imaging of brain edema in the neonatal rat: a comparison of short and long term hypoxia-ischemia. Pediatr Res. 38:113–118.

Rumpel H, Nedelcu J, Aguzzi A, Martin E. 1997. Late glial swelling after acute cerebral hypoxia-ischemia in the neonatal rat: a combined magnetic resonance and histochemical study. Pediatr Res. 42:54–59.

Sbarbati A, Pizzini F, Fabene PF, Nicolato E, Marzola P, Calderan L, Simonati A, Longo L, Osculati A, Beltramello A. 2004. Cerebral cortex three-dimensional profiling in human fetuses by magnetic resonance imaging. J Anat. 204:465–474.

Schmued LC, Hopkins KJ. 2000. Fluoro-jade B: a high affinity fluorescent marker for the localization of neuronal degeneration. Brain Res. 874:123–130.

Sidman RL, Rakic P. 1973. Neuronal migration, with special reference to developing human brain: a review. Brain Res. 62:1–35.

Sizonenko SV, Kiss JZ. 2004. Increased astrocytic and oligodendroglial reaction after hypoxia-ischemia in the immature P3 rat brain. Dev Neurosci. 27:249.

Sizonenko SV, Kiss JZ, Inder T, Gluckman PD, Williams CE. 2005. Distinctive neuropathological alterations in the infragranular layers of the parietal cortex after moderate ischemic-hypoxic injury in the very immature rat brain. Pediatr Res. 57:865–872.

Sizonenko SV, Mayall Y, Sirimanne E, Gluckman PD, Inder T, Williams CE. 2003. Selective cortical alteration after hypoxic-ischemic injury in the very immature rat brain. Pediatr Res. 54:263–269.
Volpe JJ. 2001. Neurology of the newborn. Philadelphia: Saunders.
Woodward LJ, Edgin JO, Thompson D, Inder TE. 2005. Object working memory deficits predicted by early brain injury and development in the preterm infant. Brain. 128:2578–2587.
Zhang J, Chen YB, Hardwick JM, Miller MI, Plachez C, Richards LJ, Yarowsky P, van Zijl P, Mori S. 2005. Magnetic resonance diffusion tensor microimaging reveals a role for Bcl-x in brain development and homeostasis. J Neurosci. 25:1881–1888.
Zhang J, Richards LJ, Yarowsky P, Huang H, van Zijl PC, Mori S. 2003. Three-dimensional anatomical characterization of the developing mouse brain by diffusion tensor microimaging. Neuroimage. 20:1639–1648.